Journal of Cleaner Production 348 (2022) 131342

Contents lists available at ScienceDirect

Journal of Cleaner Production

journal homepage: www.elsevier.com/locate/jclepro

Recycling of Ti6Al4V machining swarf into additive manufacturing feedstock powder to realise sustainable recycling goals

Sahil Dhiman [a,b,c], Ravinder Singh Joshi [a], Sachin Singh [a], Simranpreet Singh Gill [d,*], Harpreet Singh [e], Rakesh Kumar [f,g], Vinod Kumar [a]

[a] Department of Mechanical Engineering, Thapar Institute of Engineering and Technology, Patiala, India
[b] Micro Mechanics Lab, Indian Institute of Technology Hyderabad, Sangareddy, Kandi, India
[c] School of Engineering, Deakin University, Geelong, VIC, 3216, Australia
[d] Department of Mechanical Engineering, Sardar Beant Singh State University, Gurdaspur, India
[e] Department of Mechanical Engineering, Indian Institute of Technology Ropar, Roopnagar, India
[f] CSIR-National Metallurgical Laboratory, Jamshedpur, India
[g] Department of Fuel Minerals and Metallurgical Engineering, Indian Institute of Technology (Indian School of Mines), Dhanbad, India

ARTICLE INFO

Handling Editor: Kathleen Aviso

Keywords:
Recycling
Machining waste
Ti6Al4V
Additive manufacturing
Life cycle assessment
Direct metal laser sintering

ABSTRACT

This paper addresses the imperative need to develop sustainable recycle technologies for high value machining swarf generated during the processing of Ti6Al4V alloy. A novel recycling process based on multi-stage ball milling is proposed. The process converts Ti6Al4V swarf into a powder feedstock suitable for additive manufacturing (AM). The powders produced from the cleaned swarf using an in-house designed and fabricated tumbler ball mill were characterised in terms of their morphology, particle size, flowability and spreadability. It was found that the dominant effect of milling with Ø 25 mm balls was particle size reduction (up to ~ 40%) and the primary effect with smaller balls of Ø 6.25 mm was modification of particle morphology from irregular to rounded shape; thus, necessitating adoption of a multi-stage milling approach to achieve required size and morphology. Ti6Al4V powder having particle size in the range of 40–200 μm and near-spherical morphology was obtained after multi-stage ball milling up to 18 h. The powder characteristics were comparable or superior to the powder produced by generally used gas atomization (GA) process. The suitability of the powders for AM was established through direct metal laser sintering (DMLS). The proper melting of the optimally prepared powder occurs at 1000 mm/s scanning speed and 310 W of laser power. The developed multi-stage ball milling process was assessed vis-à-vis gas atomization using life cycle assessment (LCA). LCA revealed that the proposed ball milling method consumed lower energy (~59%), had lower eco-cost (~82%), and lesser global warming potential (GWP) (~68%).

1. Introduction

The United Nations Development Programme (UNDP) listed responsible consumption and production as the 12th sustainable development goal that was later adopted by the United Nations organisation member states in 2015 (Bexell and Jönsson, 2017). The efficient management of our shared natural resources and the way we dispose of toxic waste and pollutants are important targets to achieve this goal (Doaemo et al., 2021). Encouraging industries, businesses, and consumers to recycle and reduce waste by supporting countries is equally important to move towards more sustainable consumption patterns (Wiedmann et al., 2015). In this context, it is pertinent to note that large quantities of high value waste originates from titanium (Ti) processing industries (Dutta and Froes, 2015). Typically, Ti alloys find wide spread uses in applications ranging from avionics to biomedical owing to their exceptional properties such as high corrosion resistance, impact toughness, formability, weldability, and biocompatibility (Dhiman et al., 2019). The extraction of primary titanium is carried out by magnesiothermic reduction of $TiCl_4$ (Kroll process) which involves complex processing steps and, thus, results in high energy consumption and production costs (Zhang et al., 2020). Moreover, machining of Ti alloys is comparatively difficult and it generates considerable amount of waste in the form of swarf, turnings, hard waste, and agglomerated powder waste (Singh et al., 2020) (Fig. 1). It is estimated that 55% of the

* Corresponding author.
E-mail address: simranpreet@bcetgsp.ac.in (S.S. Gill).

https://doi.org/10.1016/j.jclepro.2022.131342
Received 29 January 2021; Received in revised form 11 March 2022; Accepted 11 March 2022
Available online 16 March 2022

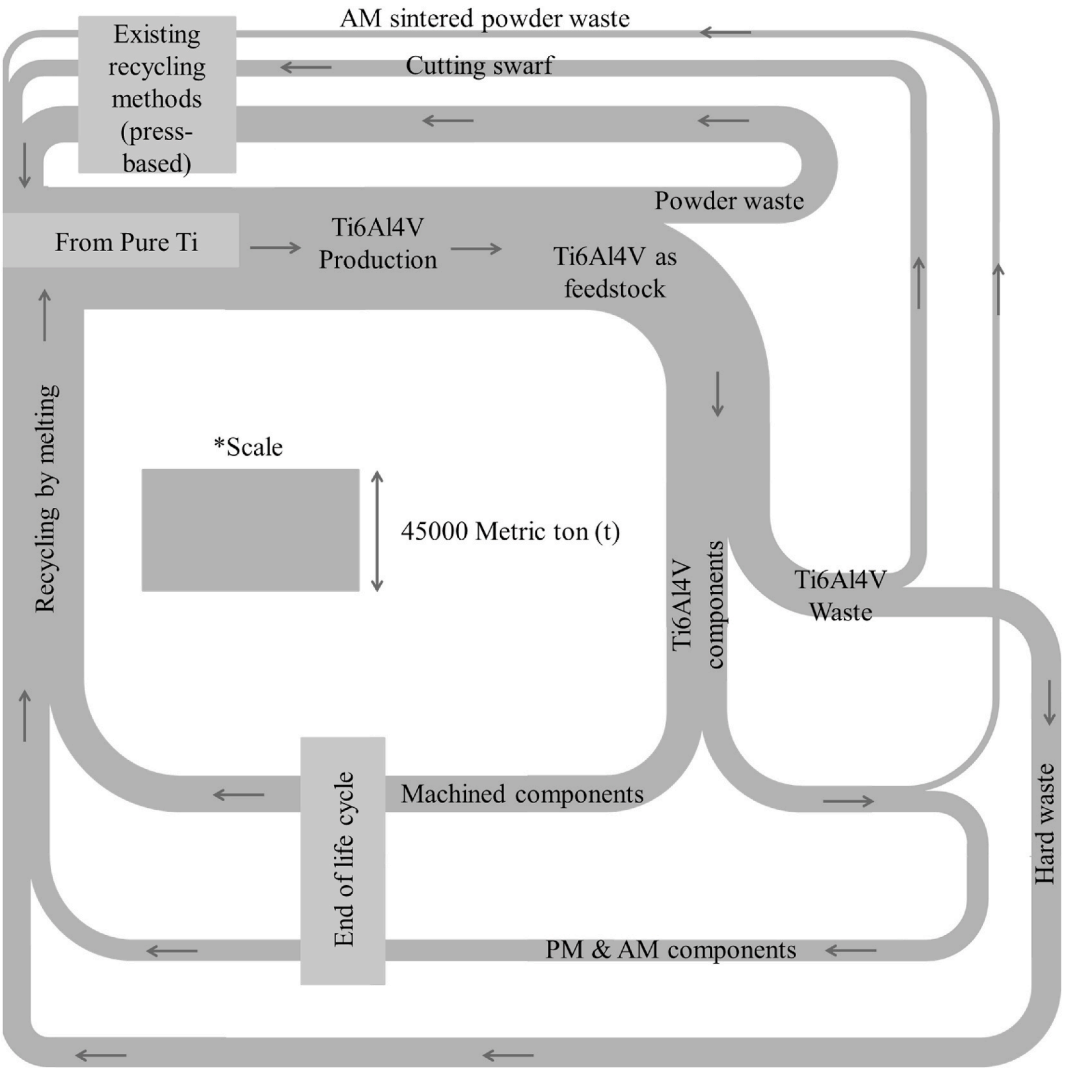

Fig. 1. Ti6Al4V life cycle shows various plausible recycling routes (data from (Goonan, 2004):).

total Ti alloy input material gets converted into machining waste (national data of US) (Goonan, 2004). Recycling of these metallic wastes is an important step towards resource conservation and, environmentally and economically sound proposition (vis-à-vis primary titanium production) provided technologically sound process(s) are available.

Conventionally, the swarf (size <1000 μm) is recycled by going through various processes: crushing, centrifuge (oil recovery), thermal degreasing, melting in furnaces, and casting into ingots (Goonan, 2004). The melting step involved in recycling has many limitations. These include: the use of water-cooled copper crucibles, energy-intensive vacuum arc melting furnaces, the requirements of vacuum and inert environment (Bomberger and Froes, 1984). Also, to achieve homogeneity in the recycled material, this process can only melt a small volume of the swarf. It has been reported that metal recycling via such routes consumes >6000 L of water per metric ton of output (Martchek, 2000). On melting, the swarf emits metallurgical smoke due to oxidation of impurities (Cirtina et al., 2016). The smoke has a high value of global warming potential (GWP) and harmful to the environment. All these issues collectively contribute to a permanent metal loss (15–25%) which leads to the unsustainability of the entire process (Rotmann et al., 2011). To overcome the shortcomings of conventional recycling, press-based recycling methods such as cold pressing (HU et al., 2012), equal channel angular pressing (Luo et al., 2012), hot extrusion (Tekkaya et al., 2009), and spark plasma sintering (Paraskevas et al., 2014) have been explored recently. Since no melting is involved, these methods require less energy input (Mahmood et al., 2012). However, these processes involving solid-state processing are reported to suffer from the problems of inferior mechanical characteristics and poor surface topography of the fabricated parts (Misiolek et al., 2012).

In recent times, alternate routes of recycling Ti6Al4V swarf (e.g. hydrogenation-dehydrogenation (HDH), ball milling route, etc) are explored to produce powders. Gökelma et al. (2018) characterized the powder produced from Ti6Al4V swarf using hydrogenation-dehydrogenation (HDH) process and further used it as feedstock in cold spray technology. Likewise, Umeda et al. (2017) recycled the coarse Ti6Al4V machining chips into fine powder using ball milling (BM) for powder metallurgy (PM) applications. The majority of the researchers explored the two-step recycling method - HDH process followed by BM to convert Ti6Al4V machining chips into powder. But the initial step, i.e., the HDH process itself is energy-intensive. It is hard to maintain specific temperature and pressure conditions during the process; also, utilization of hydrogen in a controlled environment is a challenge (Hamayun et al., 2019). Furthermore, the shape of the particles produced using HDH process is highly angular which are unsuitable for metal AM.

The metal powder feedstock for metal AM is generally produced using the gas atomization (GA) technique (Fedina et al., 2020). In this process, the metal is made to melt at high temperatures using vacuum

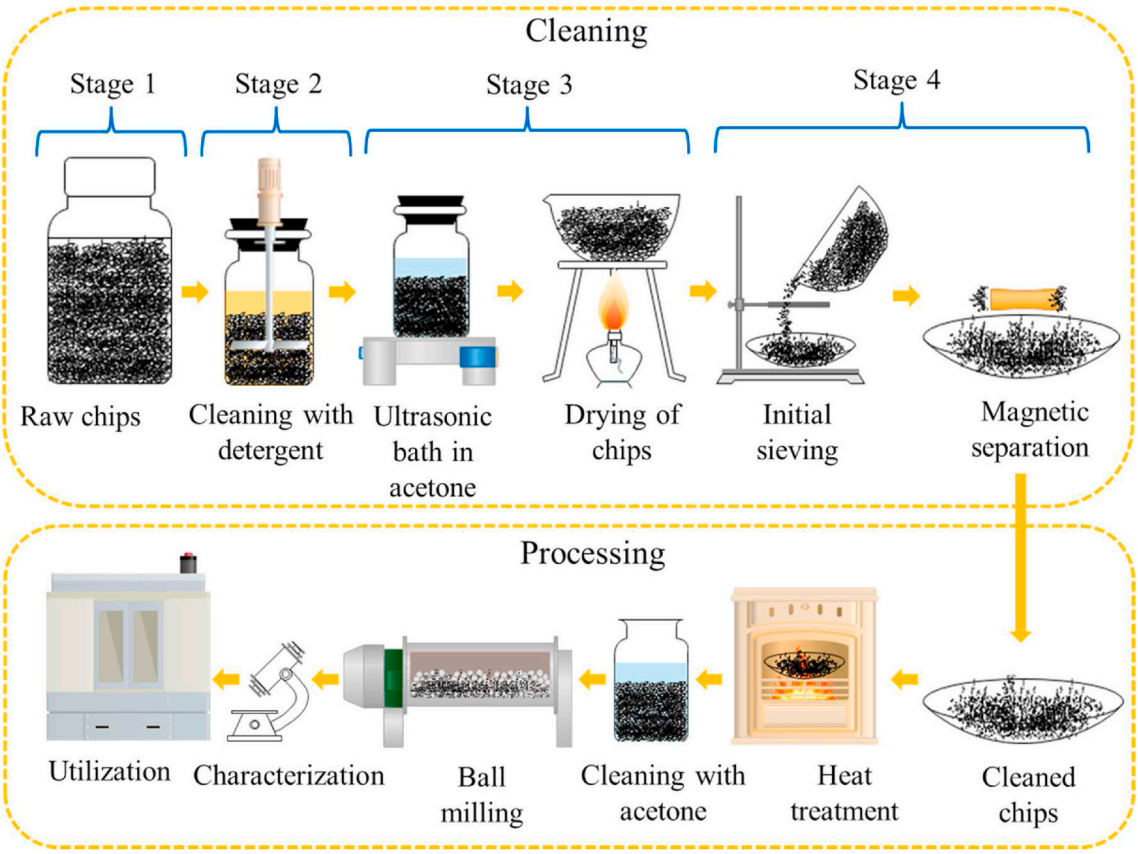

Fig. 2. Steps followed in cleaning and processing the Ti6Al4V swarf.

induction furnaces and atomized by a high-pressure (0.5–4 MPa) jet of an inert gas, such as argon and nitrogen (Abu-Lebdeh et al., 2016). The price of consumables, namely, liquid nitrogen used to cool the melted powder, high purity raw material and electricity are very high in this process (Lagutkin et al., 2004). The raw material used in the GA process is freshly procured high purity billets of the concerned material (Tsirlis and Michailidis, 2020). This entire process is energy-intensive and only feasible for mass production (Dunkley, 2013). Besides, the production of harmful metallurgical smoke during the melting of metal is not suitable for the onsite workers and the environment. Thus, the GA process is not economical and environment friendly (Dunkley, 2013) and in turn, there is a requirement to develop a clean powder production technique.

High energy ball milling (BM) is a process used to grind coarse powders into a fine homogeneous mixture of metals, alloys, or composites (Sopicka-lizer, 2010). It comprises of a rotating vial containing metal/ceramic balls along with a coarse mixture of raw material. The rotation of the vial makes balls interact with powder, and by abrasion and impact phenomenon, the morphology and size of the particle changes (Suryanarayana, 2001). (Baláž, 2021) and (Dhiman et al., 2021) have comprehensively reviewed the use of ball milling in the recycling of metallic wastes. Ball milling is explored for the machining chips of aluminium alloys (Canakci and Varol, 2015; Fuziana et al., 2014; Rosso et al., 2013), copper alloys (Afshari and Ghambari, 2016; Prem et al., 2015), stainless steel (de Sales Pereira Mendonça et al., 2018; Enayati et al., 2007; Mendonça et al., 2018), and titanium alloys (Mahboubi Soufiani et al., 2010)). In recent papers (Fullenwider et al., 2019a) and (Fullenwider et al., 2019b), impact of ball size has been explored in the recycling of stainless steel chips and powders of required characteristics were produced. Similarly (Abdollahi et al., 2013), produced grey cast iron powder from grey cast iron scraps using high-energy milling process.

Literature on the recycling of titanium alloy wastes by ball milling is scanty. The key objective of this study is to bridge this gap and develop a clean process to convert Ti6Al4V swarf into powder feedstock by BM without using the hydrogenation-dehydrogenation (HDH) step. The swarf generated during the hacksaw-driven cutting of Ti6Al4V billets which contains worn out blade material and coolant as impurities is used. The novel feature of the process is to use multi-stage ball milling where the milling energy is varied by changing ball size (Kwade, 1999). The produced powders are characterised in terms of morphology, particle size, flowability and spreadability. The suitability of the powders for intended application in AM is established through direct metal laser sintering (DMLS). The life cycle analysis of the developed ball milling process is carried out to establish its superiority vis-à-vis well-established gas atomization (GA) process.

2. Material and methods

2.1. Preparation of Ti6Al4V swarf for ball milling

Ti6Al4V swarf obtained from cutting operation of billets using steel blade was acquired from Bhagyashali Metal Industries (Mumbai, India). It was cleaned and processed as per the schematic shown in Fig. 2. First, the coolant impurities were removed by washing with detergent followed by cleaning in the sonicator for 1 h. The cleaned swarf was then dried and sieved to eliminate very large particles (>1000 μm) and foreign impurities that could interfere with the final results. Magnetic separation was carried out to remove the steel impurity of the cutting blade. Post this, heat treatment (2 h at 800 °C) in a vacuum furnace was performed to thermally decompose any leftover impurity. Finally, before BM, cleaning was done with acetone to remove any residue left behind after the vacuum furnace treatment.

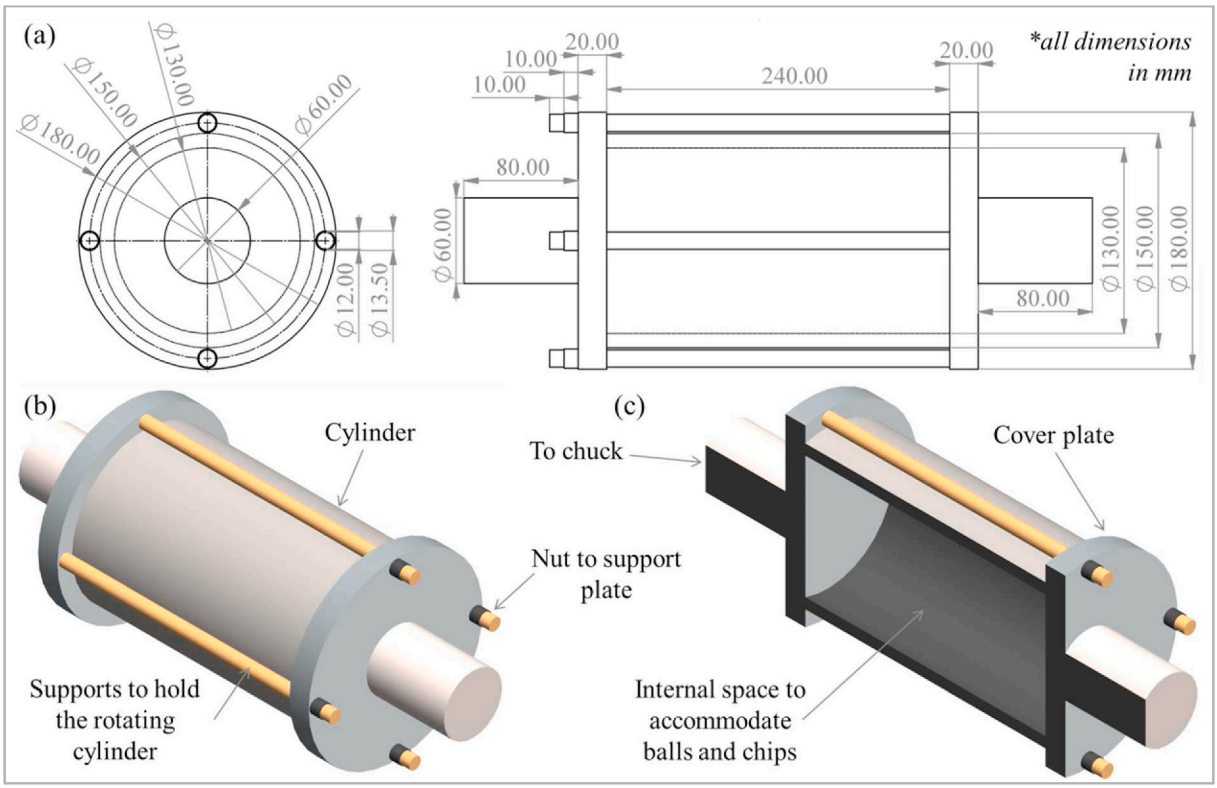

Fig. 3. Specifications of In-house designed and fabricated tumbler ball milling apparatus.

Table 1
Ball milling parameters employed for the conversion of Ti6Al4V swarf into powder feedstock for additive manufacturing.

S.No.	Sample code	Stage	Ball dia. (mm)	Milling time per stage (h)	Total Milling time (h)	Milling energy change (with respect to Ist stage)		
						SI	SN	E_m
1.	1S–6H	I	Ø 25	6 (2-2-2)	6	1	1	1
2.	2S–12H	II	Ø 12.5	6 (2-2-2)	12	0.12	7.6	0.9
3.	3S–18H	III	Ø 6.25	6 (2-2-2)	18	0.014	44.7	0.6

2.2. Ball milling of prepared swarf

The cleaned Ti6Al4V swarf was milled using an in-house fabricated tumbler ball mill driven by a CNC lathe machine (model: SANDS Precision SLT-135). The design specification of the BM is shown in Fig. 3. It consisted of a stainless-steel cylindrical jar with an internal diameter of 130 mm, a wall thickness of 10 mm, and an inside volume of 12742.30 cm^3. For Ti6Al4V alloy, the ball diameters were selected from a study by (Mahboubi Soufiani et al., 2010). Milling balls of stainless steel having a diameter of 25 mm (Ø 25), 12.5 mm (Ø 12.5), and 6.25 mm (Ø 6.25) were used. The milling media with a consistent 20:1 BPR (weight ratio) was maintained throughout the BM operation. The cylindrical jar was sealed to avoid excessive oxidation of the powder. It was rotated at 73, 70, and 68 rpm (for Ø 25, Ø 12.5, and Ø 6.25 respectively, which corresponds to 80% of critical speed for the tumbler ball mill calculated using the formula, $C = \frac{60}{2\pi}\sqrt{\frac{g}{(R-r)}}$ (where g (9.8 m s^{-2}) is the acceleration due to gravity, R is the radius of BM cylinder (in m), and r is the radius of the respective ball (in m). Three BM conditions, referred to as 1S–6H (Stage-I), 2S–12H (Stage-II), and 3S–18H (Stage-III) (Table 1), were studied to investigate the effect of multi-stage BM on the size reduction and morphology modification of Ti6Al4V swarf. The duration of each milling stage was 6 h. The mill was paused for 30 min after every 2 h of continuous rotation to avoid overheating the media and the associated system. As indicated in Table 1, the milling conditions from Stage-I to Stage-II signify decreasing stress intensity (SI) (kinetic energy of media) and increasing stress number (SN) (probability of collision or contact area) (Kwade, 1999). Milling energy (E = SI x SN) from Stage-I to Stage-III changes in the ratio 1: 0.9: 0.6. The process starts with the BM of a fixed amount of cleaned swarf. After every milling stage, the powder (generated from the swarf) was sieved for 10 min to obtain the particle size distribution (PSD) and change in morphology. This process continued until the final stage of BM.

2.3. Characterization of ball-milled powder

PSD was obtained by sieving and weighing the powder after every 2 h of BM. The particles were separated using sieves of different mesh (sieve opening in μm): #300(53), #200(75), #106(106), #80(150), #60 (250), #44(400), #30(500), #22(710), and #16(1000). The powder in the range of 53–150 μm was considered for the examination of morphology by scanning electron microscope (SEM) (model: JEOL6610LV) equipped with energy-dispersive X-ray spectroscopy (EDS). After every stage, the powder was taken and mounted in epoxy for further characterization. It was then polished using a standard metallographic procedure. The hardness of the powder particles was measured using Vickers microhardness tester (model: Wilson 402MVD, US) at 100 gf load for 10 s. Oxygen pickup was measured by EDS analysis after every stage. For the hardness and oxygen pickup measurements, an average of three readings was taken to eliminate any inconsistency. The

Table 2
Parametric design for the utilization of prepared powder by direct metal laser sintering (DMLS).

S.No.	Powder code	Laser power, LP (W)	Scanning speed, SS (mm/s)
1	3S–18H	250	1000
2	3S–18H	250	1300
3	3S–18H	310	1300
4	3S–18H	310	1000

flowability of the bulk powder was examined using the angle of repose (α) measurement as per ASTM B964-16 (standard test technique for metal powder flow rate using the Carney funnel). Spreadability was analysed using the method proposed in the study by (Ahmed et al., 2020).

2.4. Utilization of produced powder in DMLS

The powder obtained after BM was used to fabricate single tracks (one layer of powder melted by laser beam) using the DMLS system (model: EOSINT M280). The 3S–18H (Stage-III) powder was used to generate single tracks as per the parametric design shown in Table 2. These are pre-optimised commercially used parameters for the Ti6Al4V alloy for a particle size ranges from 50 to 150 μm having spherical morphology (Vaglio et al., 2020). The constant parameters include a laser spot size of 80 μm and a layer thickness of 100–140 μm.

2.5. Evaluation of single tracks fabricated by DMLS

The powder in the range of 53–100 μm was used for the fabrication of single tracks. The powder layer thickness of 100–140 μm was spread manually on the Ti6Al4V base plate. The laser then scanned a length of 1 cm to obtain single tracks, as shown in Fig. 4. Using SEM, the single tracks were characterised in terms of continuity, track width, porosity, and defects. Also, the hardness of the single tracks was measured using nanoindenter (model: Hyistron TI 950) with a 5 mN load by taking an average of three readings as the final value.

3. Results and discussion

3.1. Analysis of Ti6Al4V swarf

Characterization of the as-received Ti6Al4V swarf was performed to ascertain its quality. The morphology and composition of the freshly procured swarf are shown in Fig. 5. It can be seen from the SEM micrograph that the chip size varies from 10 to 1000 μm. The morphology of the chips is irregular, with a dominant amount of long and thin chips. Different cutting cycles with the hacksaw blade produce the variation in chip size and morphology. Initially, the blade erodes the Ti6Al4V billet resulting in thin and small chips. Once the blade is entirely inside the billet, long and thick chips are generated. EDS mapping of Ti6Al4V swarf reveals, as expected, co-association of Ti–Al–V.

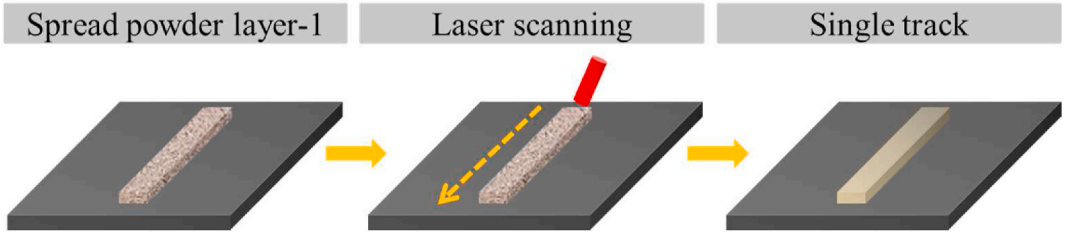

Fig. 4. Steps to generate single tracks of the prepared powder using a laser in direct metal laser sintering.

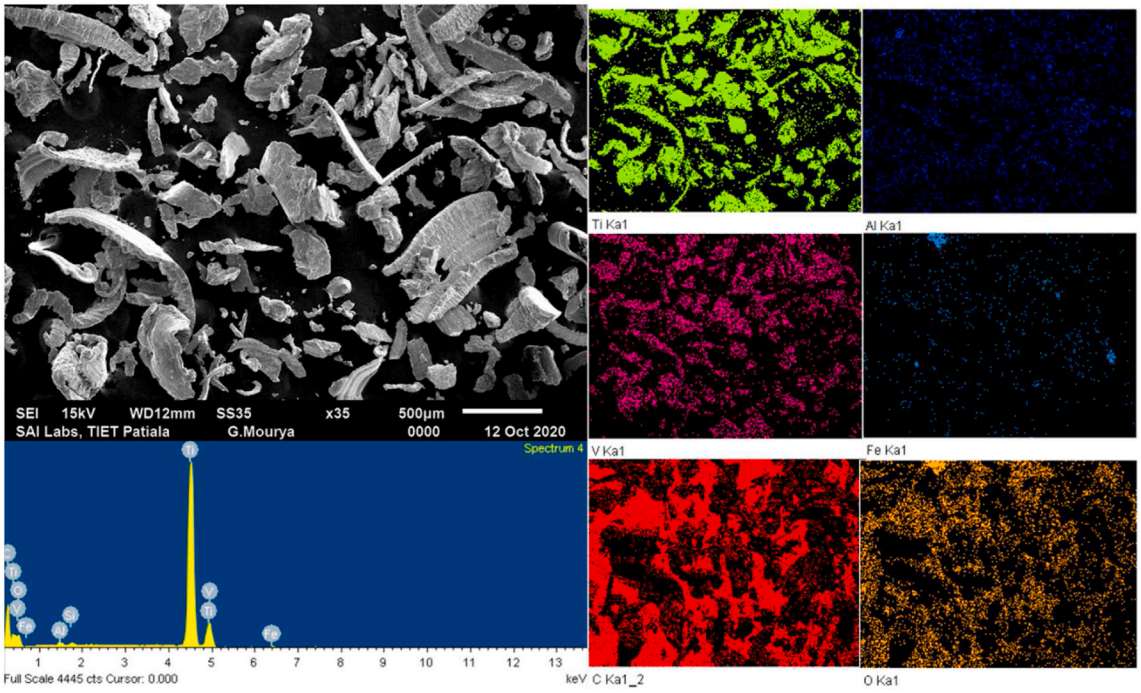

Fig. 5. Result of scanning electron microscopy and energy-dispersive X-ray spectroscopy analyses representing morphology and composition of Ti6Al4V swarf, respectively.

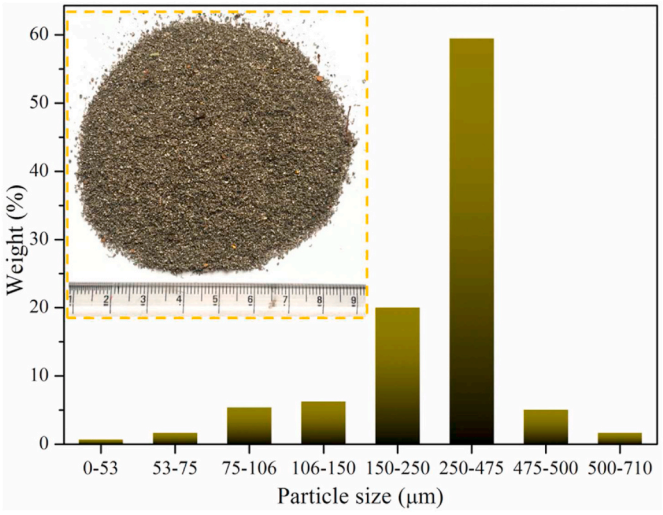

Fig. 6. Particle size distribution of cleaned Ti6Al4V swarf.

The presence of a small percentage of iron (Fe) impurity, as isolated particles due to wear of hacksaw blade is indicated. Particle size distribution of swarf is shown in Fig. 6. It can be seen that the majority of the chip particles have a size in the range of 250–475 μm.

3.2. Composition of swarf

Fig. 7 shows the elemental composition of the swarf after every cleaning stage. It can be observed that first stage cleaning leads to the removal of lubricant oil, which is shown by a decreased carbon content value (2.77 wt %). Also, a 0.18 wt % reduction in the share of Si is observed due to the soluble nature of Si and lubricant oil in detergent water. Second stage leads to the further removal of Si (0.78 wt %). After magnetic separation, removal of iron content from 1.93 to 0.06 wt % is obtained. After final cleaning with acetone, the following composition of swarf (in wt. %) was as achieved: Ti - 85.3, Al - 4.4, and V - 3.

3.3. Characterization of ball-milled powder

3.3.1. Particle size and morphology

Fig. 8 shows the effect of BM time on the size of particles. It can be seen from the PSD graphs that the particle size gets substantially modified with Ø25 balls followed by Ø 12.5 balls. The effect of Ø 6.25 balls is insignificant. This trend in reduction of particle size may be correlated with decrease of stress intensity (SI) (kinetic energy of media (Kwade, 1999)) in the mill. As compared to Ø 25 balls, there is ~98% reduction in stress intensity when Ø 6.25 balls are used. Size reduction by large size ball is due to the high impact produced by balls dropping from near the top of the shell during rotation (Fullenwider et al., 2019b).

Typical SEM micrographs in Fig. 9 shows modifications in the morphology of particles after different ball milling stage/intervals. In

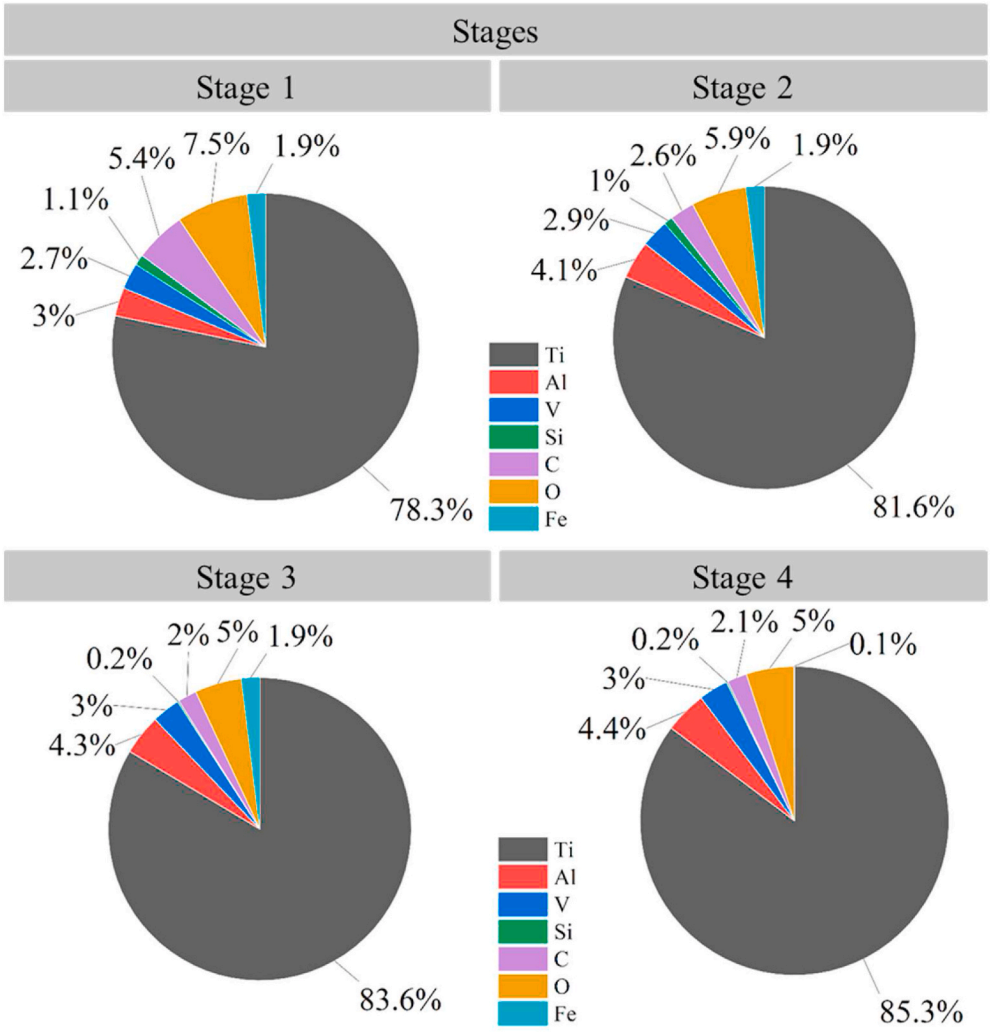

Fig. 7. Elemental composition of Ti6Al4V swarf after every cleaning stage.

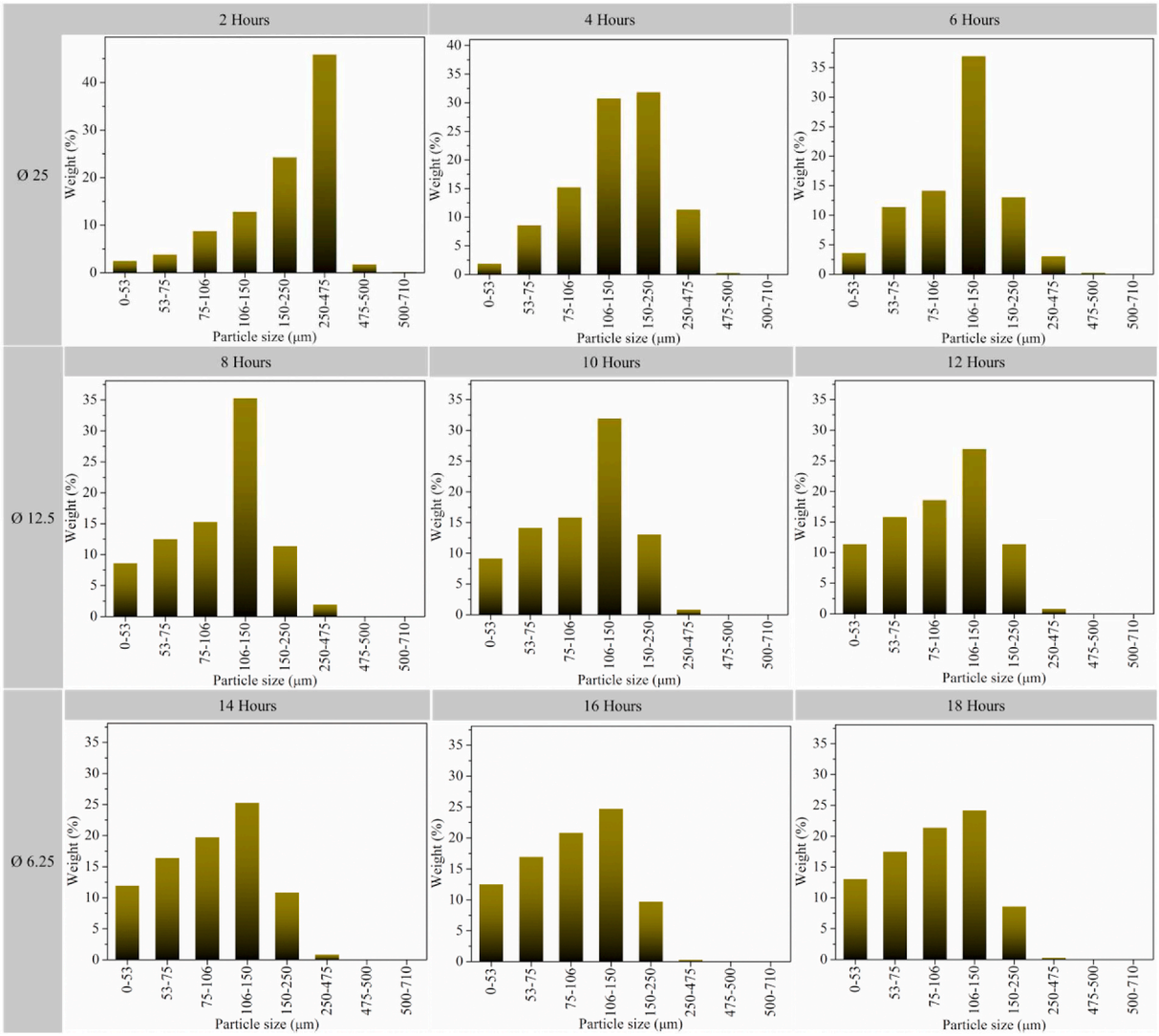

Fig. 8. Particle size distribution graphs show the effect of ball milling time and ball diameter on the particle size.

line with PSD results, the reduction in size with Ø 25 balls (sample 1S–6H) is evident from the micrographs. A notable feature in the micrographs is rounding of particles with a decrease in balls size; this feature becomes quite noticeable in the Stage-III milling (sample 3S–18H). A plausible explanation for this can be presented in terms of dominating milling mechanism, impact and abrasion as shown in Fig. 10. With large size balls, the impacts appear to induce micro-cracks become sites of crack propagation (point 4 in Fig. 10). The change from irregular morphology to rounded particles (Stage-II and III) appears to be due to increasing contribution arising from abrasion and adhesion of particles as they become finer. Herein, the balls revolve and rub hard against the wall along with the particles in between and modify their morphology (points 1, 2, and 3 in Fig. 10). Further, the stress number (SN) (Table 1) (i.e., the probability of collision or contact area between balls and material) increases ~ 15 and 45-fold as the media size is reduced from Ø 25 to Ø 12.5 and Ø 6.25, respectively. Thus, the increase in the ball-material contact area favours abrasion and rounding of the particles.

It can be observed from PSD graphs (Fig. 8) that for 3S–18H powder, the fraction of particles in the size range 53–150 μm is ~60% which is typical for commercial gas atomized (GA) powder used in DMLS. The size fraction is also comparable GA powder (~70%) (Malỳ et al., 2019). As discussed later (section on LCA analysis), the powders produced by multi-stage ball milling have an edge over GA powders in terms of cost and environmental impact associated with the production process. Particles having a size >150 μm (~8%) can further be milled to bring their size down to the desired range. In addition, the powder <50 μm (~13%) can be employed in other applications such as cold spray-based AM where a smaller size (<38 μm) is required (Singh et al., 2019).

3.3.2. *Hardness and XRD analysis*

Fig. 11 shows the variation of Ti6Al4V powder hardness with milling time. Raw swarf of Ti6Al4V (represented by 0 on the abscissa in Fig. 11) was found to have a hardness of 390 ± 4 HV. It can be seen that the hardness value increases linearly with an increase in milling time up to 440 ± 2 HV. This increase in hardness is attributed to the enhanced dislocation density and reduced grain size by work hardening due to the constant hammering action on trapped particles between balls and BM cylinder (Xu et al., 2017). As per the Hall–Petch relationship, constant hammering leads to grain refinement, which is an effective strengthening mechanism (Naik and Walley, 2020). After a saturation state (~440 HV), no further strain gets developed in the particles due to the increased plastic deformation resistance. The particles at this stage cease to deform plastically, and thus the hardness curve gets flattened with a change in morphology to near-spherical. Beyond the expected strain hardening due to BM, the oxygen pickup by Ti6Al4V also affects the hardness value (Donachie, 2000). Ti (commercially pure) has a high affinity towards oxygen, but its alloy Ti6Al4V picks up comparatively

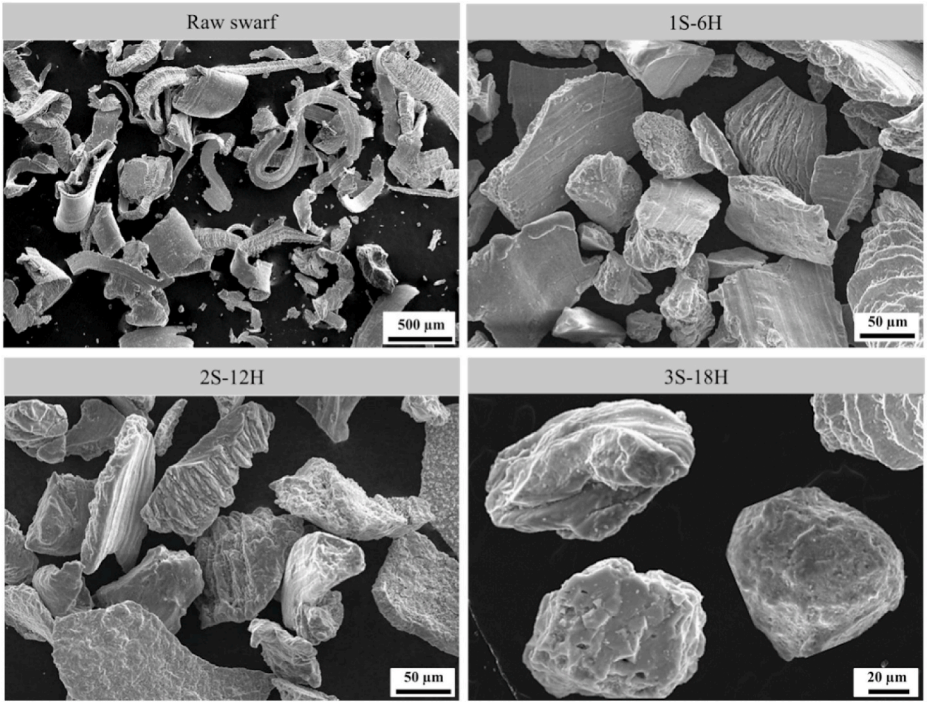

Fig. 9. Modifications in the morphology of particles after different ball milling intervals.

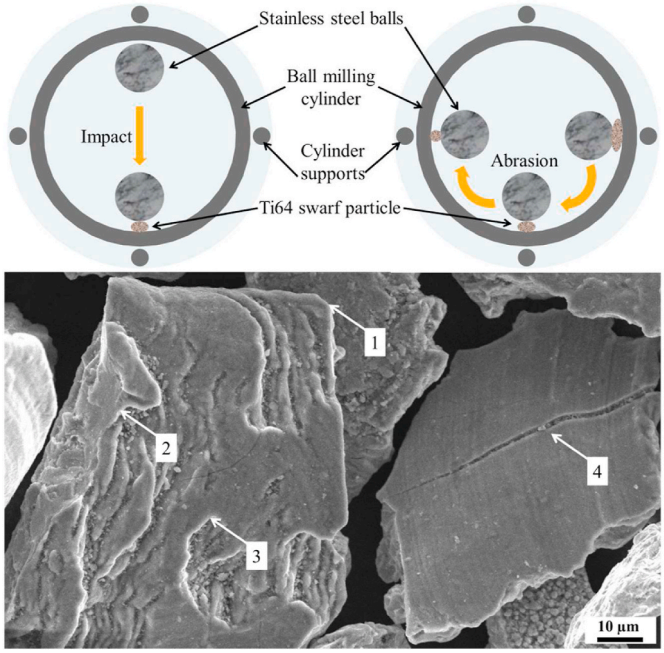

Fig. 10. Impact and abrasion action during ball milling of Ti6Al4V swarf.

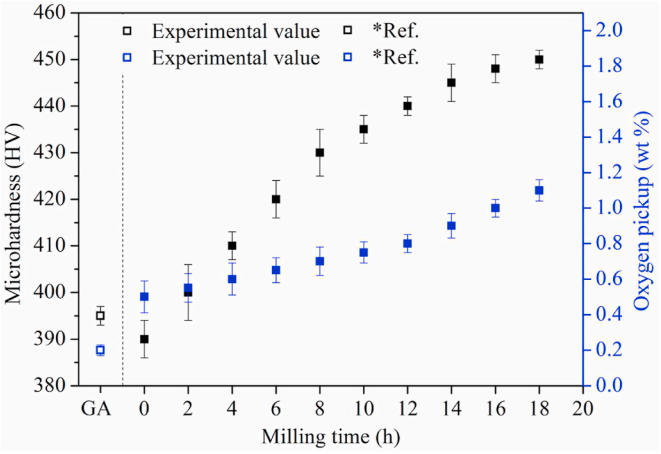

Fig. 11. Variation of hardness and oxygen pickup of ball-milled powder with milling time (*hardness (Murr et al., 2009), *oxygen pickup (Konečná et al., 2019)).

less oxygen during mechanical deformation. An increased oxygen content (from 0.5 ± 0.09 (wt %) to 1.1 ± 0.08 (wt %) till the last stage) with milling time can be seen in Fig. 11. A steep curve can be observed after 12 h because particle size cannot be reduced further except the modification in morphology which exposes a high surface area (Velasco--Castro et al., 2019). In actual operation, the oxygen pick-up can be minimized by milling in an inert atmosphere or vacuum.

Fig. 12 shows the X-ray diffraction (XRD) patterns of raw swarf, final BM powder (3S–18H), and GA powder for comparison purposes. The XRD pattern of 3S–18H powder does not reveal any extra peak for Fe due to the removal of Fe impurity during the cleaning stage. For the same powder, after the BM for 18 h, the intensity of the peaks reduced as compared to the GA powder. This loss in intensity is due to the refining of coherent scattering regions (grain size) and internal strain accumulation (Naik and Walley, 2020).

3.3.3. Powder flowability and spreadability

The measurement of α gives an idea about the cohesiveness between particles and hence the flowability. Values fewer than 30° suggest lower cohesiveness or high flowability. Higher values up to 55° indicate an increase in cohesiveness or a decrease in flowability. Over 55°, the cohesiveness is so significant that it makes powder difficult to flow properly (Carr, 1965). It can be seen from Fig. 13 that the value of α for 3S–18H powder is closer to that of GA powder. This is due to the near-spherical morphology of the 3S–18H powder that enhances its

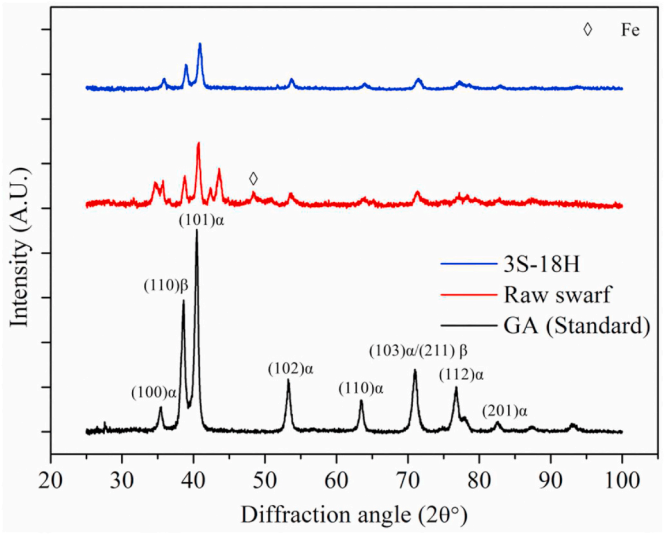

Fig. 12. X-ray diffraction patterns of Ti6Al4V raw swarf, ball-milled powder (3S–18H), and commercially available gas atomized powder.

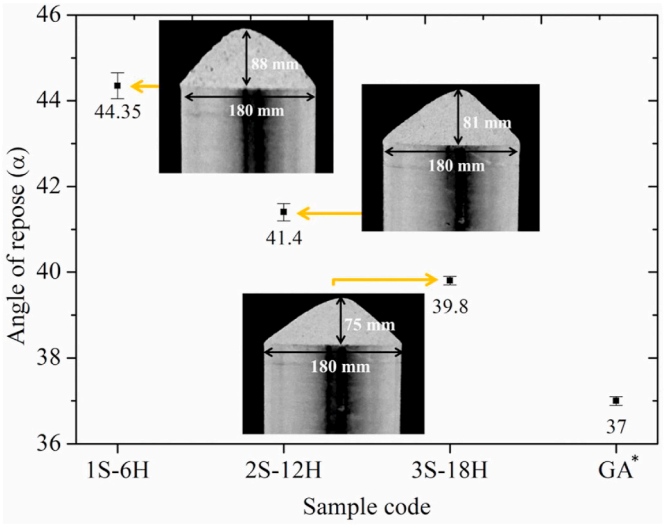

Fig. 13. Flowability results of ball-milled powders using Carney funnel (*GA (Gökelma et al., 2018)).

flowability. The particles with such morphology do not resist flow due to very little friction between them at the microscopic level. This reduction in friction is due to the absence of surface asperities (Zegzulka et al., 2018). The low flowability of the 1S–6H and 2S–12H powders is due to the angular, sharp-edged morphology of the particles (Fig. 9) as oppose to the more rounded particles in 3S–16H.

Spreadability deals with powder flow in the narrow clearances with a tiny shearing zone (Ahmed et al., 2020). The powder is usually spread on the base plate using either roller or blade with small gaps in the range of 50–150 μm depending upon the system. In the present case, due to the large size range of particles compared to GA powder, the layer thickness varies with particle size and morphology. Patchy coverage of the powder affects the particle bonding during the melting and hence affects the part quality (Townsend et al., 2016). Fig. 14 shows the spreadability analysis of the different powders produced using BM. It can be observed from the analysis that 3S–18H powder shows better spreadability in terms of the homogeneous spread of layer without patchy coverage. This is due to the near-spherical and more homogeneous morphology than 2S–12H followed by 1S–6H. The spread is inconsistent and patchy for 1S–6H due to the presence of sharp-edged particles (point 1 in Fig. 14). Moreover, the layer height is not the same throughout (points 2 and 3 in Fig. 14) because in 3S–18H powder, the share of smaller particles i.e., <106 μm is large as compared to 1S–6H. Thus, due to this, the particle accumulates in two layers (one over another). On the other hand, for 1S–6H, a high share of larger particles hinders the formation of the double layer.

3.4. Evaluation of fabricated single tracks

It can be observed from Fig. 14 that the spread of 3S–18H powder is homogeneous due to the near-spherical morphology and can generate a single layer in the DMLS system, in which only one layer per scan is melted. Thus, the only 3S–18H powder was considered suitable for further processing with the DMLS system based on the morphological, mechanical, and spreadability analyses. The results of the parametric investigation of the single tracks are shown in Fig. 15. It can be seen from Fig. 15 that both the parameters *viz.*, laser power (LP), and scanning speed (SS) are crucial to study the melting behaviour of metal powder using lasers. It is evident from trials no. 1 and 2 that at high SS, the powder did not melt appropriately due to the insufficient laser exposure time. With a high SS, a considerable fluctuation in melt pool length leads to improper melting. The effect of LP can be observed by comparing trials no. 1 and 4. The increased width of the single track can be seen with a high LP due to the large melt pool. This effect is attributed to more melting at the same SS. Due to the formation of keyholes in the melt pool caused by the non-spherical morphology of the powder, the melt pool becomes unstable that prevents the proper development of single tracks (Shrestha and Chou, 2018). However, on comparing, an

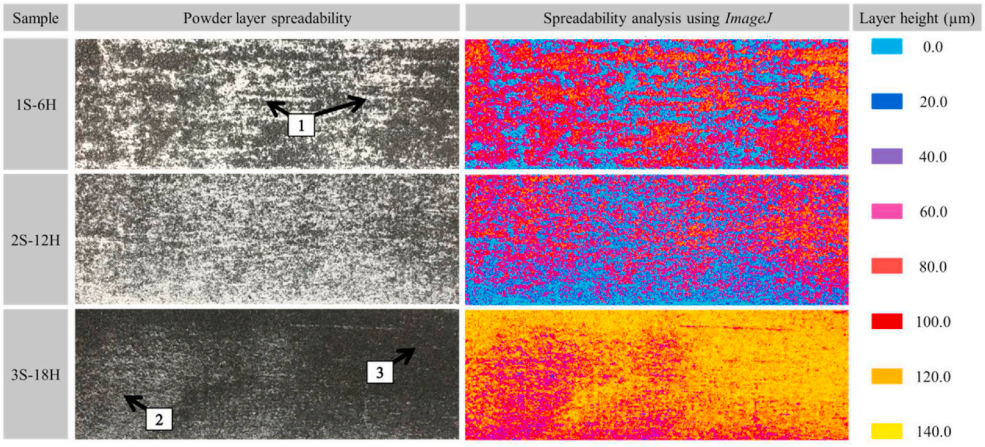

Fig. 14. Spreadability analysis of powder obtained after different stages of ball milling.

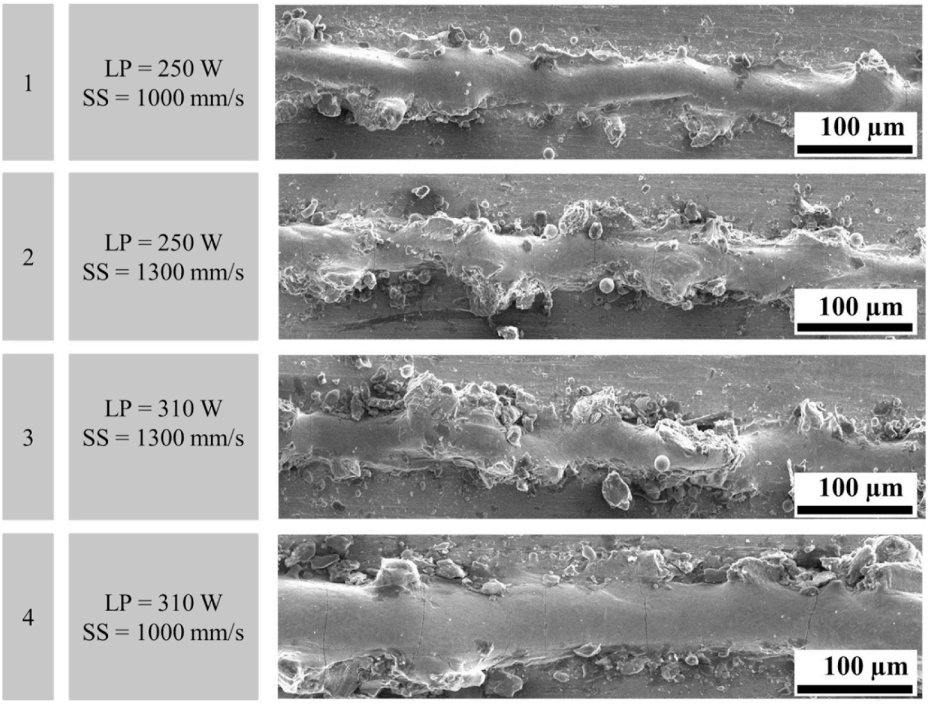

Fig. 15. Utilization of ball-milled powder (3S–18H) to fabricate single tracks by direct metal laser sintering.

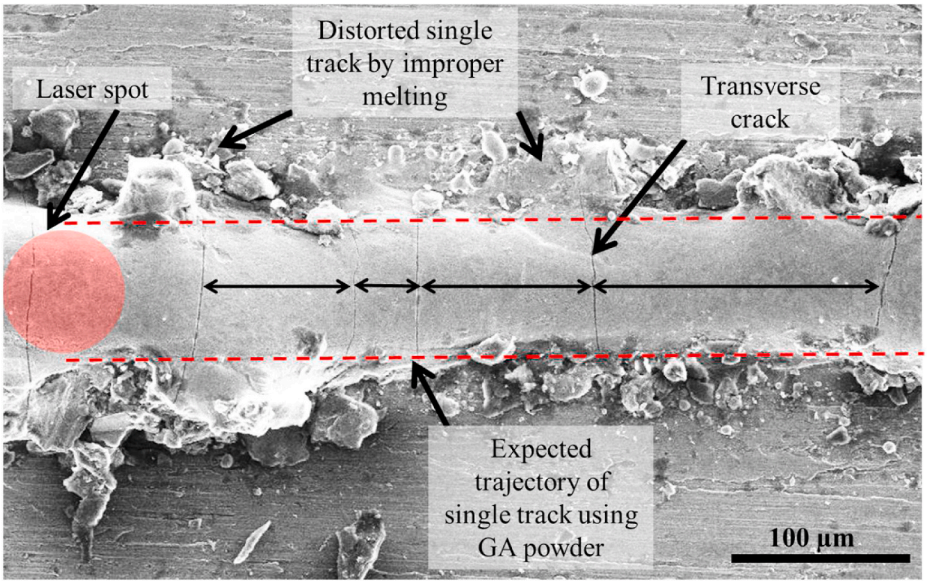

Fig. 16. Porosity and defects information in single tracks fabricated by direct metal laser sintering (red dotted lines shows single tracks width fabricated using GA powder at same parameters (Vaglio et al., 2020)).

overall uniformity in the single track can be observed in the trial no. 4. Thus, process parameters in trial no. 4 become suitable for 3S–18H powder while processing using DMLS.

Porosity and defect information of the single tracks shows that the powder is not melted properly along the length of the single track, leading to a disturbed melt pool and hence non-uniform build (Fig. 15). Also, transverse cracks were identified along the length of single tracks (Fig. 16, fabricated at SS of 1000 mm/s and an LP of 310 W, pre-optimised parameters for spherical GA powder in the same size range). Such behaviour can be justified by the material embrittlement due to oxygen. As only one single layer was deposited, after melting, the oxygen content of powder comes on surface of the printed surface in the form of oxide layer (Velasco-Castro et al., 2019). Also, the formation of a complex stress field by uneven heating and cooling process caused by the non-spherical 3S–18H powder in the DMLS process leads to these cracks.

Thus, as also suggested by (Gao et al., 2019), inadequate melting along the length and transverse cracks can be prevented by preheating the base plate (to avoid the sudden temperature variation during melting) and optimizing the total energy density required to melt 3S–18H powder.

Fig. 17 shows a comparative analysis of single tracks based on their physical and mechanical properties fabricated with 3S–18H and GA powder. For 3S–18H powder, it can be observed that with an increase in

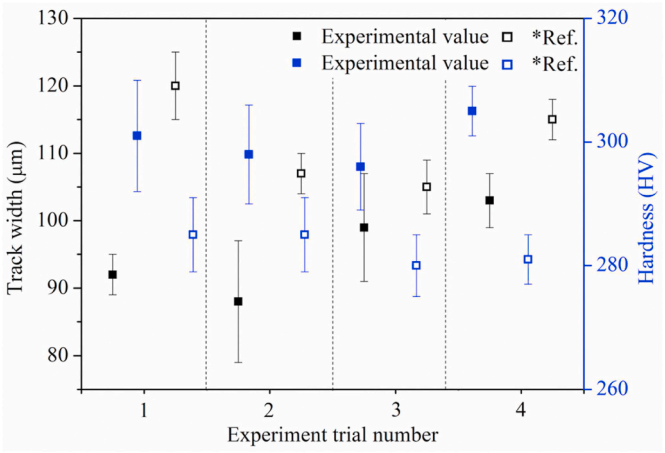

Fig. 17. Track width and hardness results by varying laser parameters for 3S–18H powder (*track width and hardness data of single tracks generated using gas atomized powder at same parameters (Vaglio et al., 2020)).

SS (trial 1 and 2), the track width decreases (~4%) but with an increase in LP (trial 2 and 3), track width increases (~10%). On the other hand, at the same parameters, with GA powder, a similar trend can be observed but with a 5–25% difference in track, width compared to the experimental values. Conversely, the overall hardness of single-track build with 3S–18H powder is better (~4–7%) than the single tracks generated with GA powder at the same parameters. But there is no particular trend in hardness values in different trials that suggests its dependency on the used parameters during DMLS.

4. Sustainability analysis

Sustainability analysis is an important strategy that defines the success factor by comprehending its impact on the environment and cost to the industry (Dimian et al., 2014). For the current study, LCA was used as the tool to measure the environmental impact. The associated cost of the process was also presented to provide an in-depth comparison with the GA process.

4.1. Comparative LCA study

4.1.1. Goal and scope of the study

The goal of the present LCA study was to understand and compare the environmental impact of the proposed multi-stage ball milling process with its conventional counterpart, GA. The scope of the study was limited to the production of powder via these two different routes. There are general assumptions made for the present LCA study. These include: (a) both the processes were considered as continuous operation, i.e., neglecting the initial material and energy wastage; (2) electricity used for both the processes was produced from black coal (Mittal, 2010); (3) the GWP and eco-cost of Ti6Al4V swarf were taken as zero because it is a by-product generated during the preparation of Ti6Al4V billets; (4) both the processes were considered to be operated at the optimised set of parameters for the chosen raw material; (5) the study does not include the transportation share of raw and produced materials; and, (6) it also does not include the establishment cost of equipment and systems.

4.1.2. Functional unit and system boundary

The functional unit for the present study was defined as the total powder produced from 0.1 kg total weight of raw material (Ti6Al4V) (Wilson et al., 2013). This small amount of raw material was chosen due to the capability of designed BM equipment used in the present study that processes a small amount of powder in a single batch. For both the processes, the system boundaries were defined as per the cradle-to-gate variant of LCA and is shown in Fig. 18. The rationale for choosing the cradle-to-gate variant is due to the nature of the assessment, which is a partial product life cycle from the resource extraction (cradle) to the factory gate, just before it is transported to the consumers (gate).

4.1.3. Life cycle inventory analysis

The primary data (BM, heat treatment, and cleaning) was collected

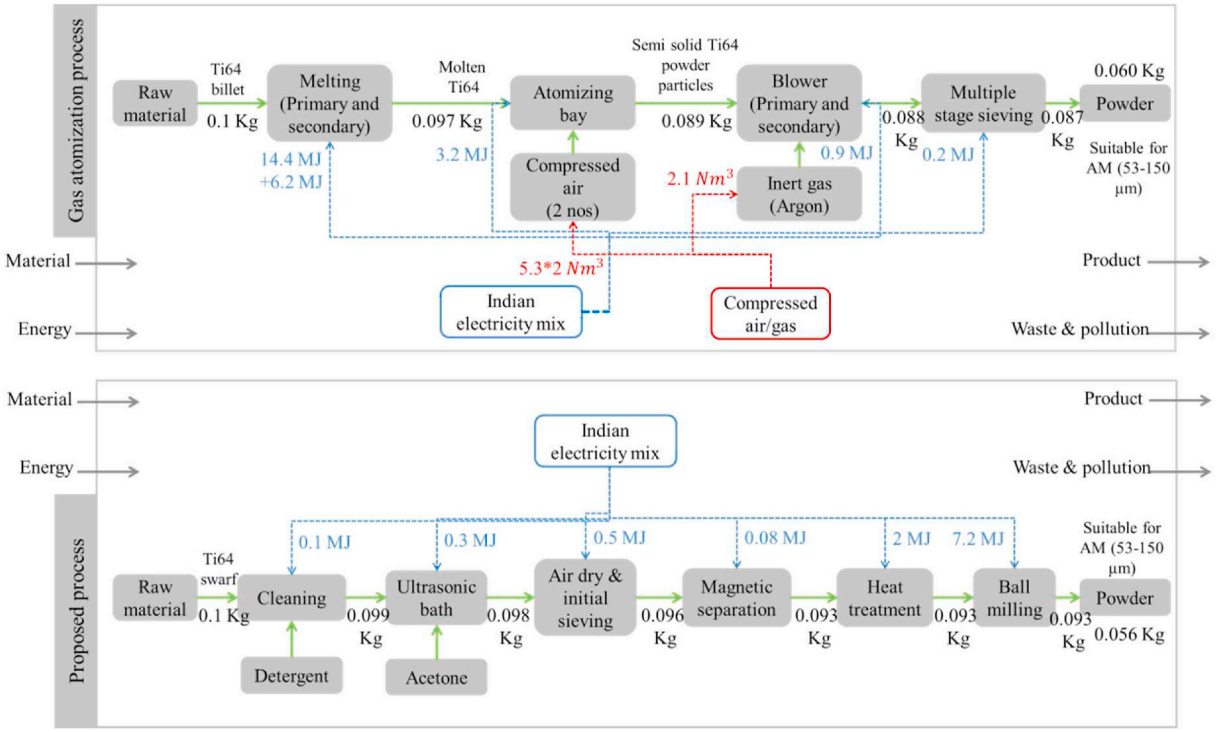

Fig. 18. System boundaries for gas atomization and proposed process.

Table 3
Inventory data used in comparative life cycle assessment study.

Gas atomization process				
S. No.	Energy/material	Unit	Quantity	Reference
1	Ti6Al4V billet	kg	0.1	Kept fixed
2	Electrical energy for Ti6Al4V melting (primary and secondary)	MJ/0.1 kg Ti6Al4V billet	(11.4 + 6.2) = 20.60	Norgate et al. (2004)
3	Electrical energy for other processes	MJ/0.1 kg Ti6Al4V billet	4.31	TU Delft (2020)
4	Compressed air (>10 bar)	Nm^3/0.1 kg Ti6Al4V billet	5.3 × 2 = 10.62	(Sharma et al., 2020) (Ünal, 1990)
5	Inert gas (argon)	Nm^3/0.1 kg Ti6Al4V billet	2.10	Norgate et al. (2004)
Proposed method				
1	Ti6Al4V swarf	kg	0.1	Kept fixed
2	Electrical energy for BM of Ti alloys (size reduction from 400 to 10 μm)	MJ/0.1 kg Ti6Al4V swarf	7.22	Calculated and adjusted with (Pourghahramani, 2006)
3	Electrical energy for other processes	MJ/0.1 kg Ti6Al4V swarf	2.98	Calculated
4	Acetone	l/0.1 kg Ti6Al4V swarf	0.2	Calculated
5	Detergent (liquid)	l/0.1 kg Ti6Al4V swarf	0.005	Calculated
6	Water for cleaning	l/0.1 kg Ti6Al4V swarf	0.5	Calculated

Table 4
Environmental impact assessment (data taken from open-source database Idemat (TU Delft, 2020)).

S. No.	Energy/ material	GWP (kg CO_2 equivalent)	Eco-cost (external cost includes the preventive cost of human toxicity, resource depletion, and eco-toxicity)
1	Ti6Al4V billet	4.46/kg	84.30 INR*/kg
2	Indian electricity mix	0.93 kg/kWh	214.80 INR/100 MJ
3	Compressed air	0.176 kg/kg	3.30 INR/kg
4	Inert gas (argon)	0.18 kg/kg	3.98 INR/kg
5	Acetone	1.40 kg/l	17.82 INR/l
6	Detergent	10.1 kg/l	103.01 INR/l

1 US $ ~ 75 INR (2021 conversion rate).

using real-time observation during the powder production for the inventory analysis. Also, the secondary data (mostly the energy sources for GA sub-processes) was taken from reports, data product catalogues, and existing literature in journals and reference books. The inventory data for both processes is shown in Table 3.

4.1.4. Life cycle impact assessment

The final and last stage of LCA is life cycle impact assessment. Environmental impact was assessed using GWP and associated eco-cost. GWP was quantified by measuring the total amount of CO_2 equivalents emitted into the atmosphere. Eco-cost gives the preventive cost of the aggregate effects of human toxicity, eco-toxicity, and resource depletion (Vogtlander, 2010). The respective data for CO_2 equivalents and eco-cost was accessed from the open-source database Idemat by (TU Delft, 2020) and is shown in Table 4.

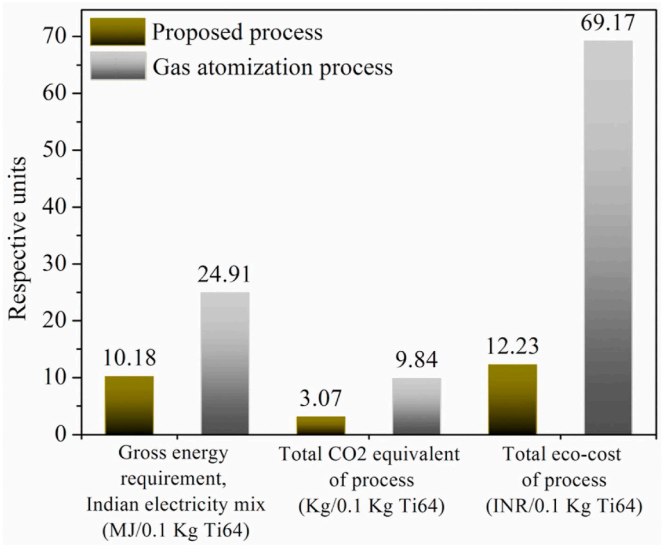

Fig. 19. Life cycle assessment results for Ti6Al4V powder produced from gas atomization and the proposed method.

4.1.5. Results of LCA

The results for the endpoint assessment are shown in Fig. 19. It can be observed from the figure that for 0.1 kg raw material, GER (Gross Energy Requirement) for the GA process is 59% more as compared to the proposed process. This huge difference in GER is primarily due to the energy-intensive melting stage (20.60 MJ/0.1 kg Ti6Al4V) in the GA process. Metallurgical smoke generated during this stage contains minute particles of metal powders and toxic substances (NO_2, silica, magnesia, calcium oxide, and alkali oxides), which are highly dangerous for living beings, and its continuous exposure can cause severe health issues (Weber, 1961). Besides, the atomization bay also consumes a significant amount of energy (3.2 MJ/0.1 kg Ti6Al4V) in the form of electricity. These stages are thus a major contributor to the GWP and total eco-cost associated with the GA process. In another LCA study on metal powders, the GWP due to energy consumption was substantially higher than any of the other associated sub-process (Tengzelius et al., 2000). A high-pressure jet of extremely pure inert gases like argon and helium is used to atomize the melted metal in the GA process (Tsirlis and Michailidis, 2020). A high value of associated GWP (0.176 kg/kg) and eco-cost (3.98 INR/kg) proved its deteriorating impact on the environment. Prolonged work in an environment having a high concentration of such gases is not safe for onsite workers (Mohankumar and Senthilkumar, 2017). However, the leftover grey-acetone in the proposed process is not a hazardous air pollutant, and microorganisms break it down in soil and water (eco-cost: 17.82 INR/l). But, the phosphates in detergents can cause freshwater algal blooms, emitting toxins and reducing oxygen levels in waterways thus, leading to its high associated eco-cost (103.01 INR/l) (Giagnorio et al., 2017). Thus, the consumption of these consumables should be minimized, and some better alternatives can be explored.

Large scale and continuous operation of the GA process is challenging to maintain due to the high cost of consumables and process constraints. Thus the total cost of the process is increased by the yield loss factor (Dunkley, 2013). As the yields can vary from 20 to 90% depending upon the scale of operation, issues such as tundish skull losses and dust losses to filters further reduce the overall yield. This leads to the high cost (25-45k INR for Ti6Al4V) of commercial powder feedstock for AM, which is not economical for large scale manufacturing (Dong et al., 2021). The total equipment cost of the GA process (1000–2000 k INR) is very high due to complex sub-systems like atomization bay and highly controlled environment chambers (Kassym and Perveen, 2020). Skilled labour is vital to run and monitor the sophisticated GA system.

Contrarily, in the proposed process, the cost of the final powder can further be reduced by shifting the processing mode from batch to continuous due to the non-utilization of expensive consumables. The yield of the proposed process is directly dependent on the size of the BM apparatus, i.e., for a fixed time interval, the output can be regulated by varying the cylinder diameter. Raw material in the form of swarf (pre-sorted in the industry) comes at a very low price than high purity billets used in GA process. Also, the absence of the melting stage, which changes the physical state of the raw material (solid to liquid), and the absence of consumables like inert gases contribute to the sustainability based on the total GWP and associated eco-cost. In addition, the plant safety is high in the case of the proposed method due to the harmless action of the BM process. More technical and scientific interventions in the proposed process will further reduce the environmental footprint of the known hotspots.

5. Conclusions

Following are the key conclusions which follows from this study:

1. Particle size and morphological changes during ball milling are dependent on the diameter of steel balls used as milling media. While size reduction and sharp-edged particles are favoured with large size balls (Ø 25 mm), the small size ball (Ø 6.25 mm) promotes morphological changes in terms of rounding of particles; thus, justifying the need to use multi-stage milling for the desired size and morphology of the product powder.
2. A plausible explanation for particle size reduction and morphological changes is presented in terms of stress intensity (kinetic energy of media) and stress number (probability of collision) which increases with decrease in ball size. For comparable milling energy, higher stress intensity favours size reduction and morphological changes are favoured at higher stress number.
3. With an increase in milling time, the hardness value of powder increases linearly (up to 430 HV) and this is attributed to the work hardening and oxygen pickup effects.
4. The characteristics of powders produced by multi-stage ball milling process, namely size, angle of repose, flowability and morphology were either comparable or superior to the commercial powders produced by gas atomization method.
5. In direct metal laser sintering (DMLS)
   a) the suitable parameters for melting powders produced after three stages of milling (3S–18H powder) are: scanning speed of 1000 mm/s and laser power of 310 W.
   b) the overall hardness of single-track built with 3S–18H powder is better (~4–7%) than the single tracks produced with GA powder under the same conditions.
6. The LCA study of developed process vis-à-vis gas atomized powders indicates superiority of the proposed multi-stage ball milling method since it consumes less energy (~59%), has low eco-cost (~82%), and has less GWP (~68%). Thus, the process has the potential to produce powders with regulated characteristics from Ti6Al4V swarf.

Funding

This research was partially funded by Swachhta Saarthi Fellowship 2021 (SSF/B/65) by the office of the principal scientific adviser to the government of India.

CRediT authorship contribution statement

Sahil Dhiman: Conceptualization, Methodology, Writing – original draft, preparation, Writing – review & editing. **Ravinder Singh Joshi:** Writing – review & editing. **Sachin Singh:** Writing – review & editing. **Simranpreet Singh Gill:** Writing – review & editing, Supervision. **Harpreet Singh:** Writing – review & editing, Supervision. **Rakesh Kumar:** Writing – review & editing, Supervision. **Vinod Kumar:** Supervision.

Declaration of competing interest

The authors declare that they have no known competing financial interests or personal relationships that could have appeared to influence the work reported in this paper.

Acknowledgments

The first author is grateful to the following people for their support: Mr. Lalit Kumar (in charge, mechanical workshop, Thapar Institute of Engineering and Technology, Patiala) for his guidance in the experimental work; Mr. Mohammed Bin Zacharia K (National Institute of Technology, Warangal) for his help with LCA. The authors would also like to thank the anonymous reviewers for their constructive comments and suggestions.

References

Abdollahi, H., Mahdavinejad, R., Ghambari, M., Moradi, M., 2013. Investigation of green properties of iron/jet-milled grey cast iron compacts by response surface method. Proc. Inst. Mech. Eng. Part B J. Eng. Manuf. 228, 493–503. https://doi.org/10.1177/0954405413502023.

Abu-Lebdeh, T.M., Leon, G.P., Hamoush, S.A., Seals, R.D., Lamberti, V.E., 2016. Gas atomization of molten metal: part II. Applications. Am. J. Eng. Appl. Sci. 9.

Afshari, E., Ghambari, M., 2016. Characterization of pre-alloyed tin bronze powder prepared by recycling machining chips using jet milling. Mater. Des. 103, 201–208. https://doi.org/10.1016/j.matdes.2016.04.064.

Ahmed, M., Pasha, M., Nan, W., Ghadiri, M., 2020. A simple method for assessing powder spreadability for additive manufacturing. Powder Technol. 367, 671–679. https://doi.org/10.1016/j.powtec.2020.04.033.

Baláž, M., 2021. Environmental Mechanochemistry - Recycling Waste into Materials Using High-Energy Ball Milling. Springer, Cham.

Bexell, M., Jönsson, K., 2017. Responsibility and the United Nations' sustainable development goals. In: Forum for Development Studies. Taylor & Francis, pp. 13–29.

Bomberger, H.B., Froes, F.H., 1984. The melting of titanium. JOM 36, 39–47. https://doi.org/10.1007/BF03339212.

Canakci, A., Varol, T., 2015. A novel method for the production of metal powders without conventional atomization process. J. Clean. Prod. 99, 312–319. https://doi.org/10.1016/j.jclepro.2015.02.090.

Carr, R.L., 1965. Evaluating flow properties of solids. Chem. Eng. 72, 163–168.

Cirtina, D., Ionescu, N., Cirtina, L.M., 2016. Environmental impact assessement related to metallurgical industry activities. Metalurgija 55, 481–484.

de Sales Pereira Mendonça, C., dos Santos Ribeiro, V.A., Junqueira, M.M., Sachs, D., Oliveira, L.A., Melo, M.de L.N.M., Silva, G., 2018. Recycling chips of stainless steel by high energy ball milling. Mater. Sci. Forum 930, 454–459. https://10.4028/www.scientific.net/MSF.930.454.

Dhiman, S., Joshi, R.S., Singh, S., Gill, S.S., Singh, H., Kumar, R., Kumar, V., 2021. A framework for effective and clean conversion of machining waste into metal powder feedstock for additive manufacturing. Clean. Eng. Technol., 100151 https://doi.org/10.1016/j.clet.2021.100151.

Dhiman, S., Sidhu, S.S., Bains, P.S., Bahraminasab, M., 2019. Mechanobiological assessment of Ti-6Al-4V fabricated via selective laser melting technique: a review. Rapid Prototyp. J. 25, 1266–1284. https://doi.org/10.1108/RPJ-03-2019-0057.

Dimian, A.C., Bildea, C.S., Kiss, A.A., 2014. Chapter 17 - sustainability analysis. In: Dimian, A.C., Bildea, C.S., Kiss, A.A.B.T.-C.A.C.E. (Eds.), Integrated Design and Simulation of Chemical Processes. Elsevier, pp. 679–702. https://doi.org/10.1016/B978-0-444-62700-1.00017-6.

Doaemo, W., Dhiman, S., Borovskis, A., Zhang, W., Bhat, S., Jaipuria, S., Betasolo, M., 2021. Assessment of municipal solid waste management system in Lae City, Papua New Guinea in the context of sustainable development. Environ. Dev. Sustain. 23, 18509–18539. https://doi.org/10.1007/s10668-021-01465-2.

Donachie, M.J., 2000. Titanium: a Technical Guide. ASM international.

Dong, Y.P., Li, Y.L., Zhou, S.Y., Zhou, Y.H., Dargusch, M.S., Peng, H.X., Yan, M., 2021. Cost-affordable Ti-6Al-4V for additive manufacturing: powder modification, compositional modulation and laser in-situ alloying. Addit. Manuf. 37, 101699 https://doi.org/10.1016/j.addma.2020.101699.

Dunkley, J.J., 2013. 1 - advances in atomisation techniques for the formation of metal powders. In: Chang, I., Zhao, Y.B.T.-A., P, M. (Eds.), Woodhead Publishing Series in Metals and Surface Engineering. Woodhead Publishing, pp. 3–18. https://doi.org/10.1533/9780857098900.1.3.

Dutta, B., Froes, F.H.S., 2015. The additive manufacturing (AM) of titanium alloys. In: Titanium Powder Metallurgy. Elsevier, pp. 447–468.

Enayati, M.H., Bafandeh, M.R., Nosohian, S., 2007. Ball milling of stainless steel scrap chips to produce nanocrystalline powder. J. Mater. Sci. 42, 2844–2848. https://doi.org/10.1007/s10853-006-1371-2.

Fedina, T., Sundqvist, J., Powell, J., Kaplan, A.F.H., 2020. A comparative study of water and gas atomized low alloy steel powders for additive manufacturing. Addit. Manuf. 36, 101675 https://doi.org/10.1016/j.addma.2020.101675.

Fullenwider, B., Kiani, P., Schoenung, J.M., Ma, K., 2019a. In: Gaustad, G., Fleuriault, C., Gökelma, M., Howarter, J.A., Kirchain, R., Ma, K., Meskers, C., Neelameggham, N.R., Olivetti, E., Powell, A.C., Tesfaye, F., Verhulst, D., Zhang, M. (Eds.), From Recycled Machining Waste to Useful Powders for Metal Additive Manufacturing BT - REWAS 2019. Springer International Publishing, Cham, pp. 3–7.

Fullenwider, B., Kiani, P., Schoenung, J.M., Ma, K., 2019b. Two-stage ball milling of recycled machining chips to create an alternative feedstock powder for metal additive manufacturing. Powder Technol. 342, 562–571. https://doi.org/10.1016/j.powtec.2018.10.023.

Fuziana, Y.F., Warikh, A.R.M., Lajis, M.A., Azam, M.A., Muhammad, N.S., 2014. Recycling aluminium (Al 6061) chip through powder metallurgy route. Mater. Res. Innovat. 18, S6-354–S6-358. https://doi.org/10.1179/1432891714Z.000000000981.

Gao, P., Wang, Z., Zeng, X., 2019. Effect of process parameters on morphology, sectional characteristics and crack sensitivity of Ti-40Al-9V-0.5Y alloy single tracks produced by selective laser melting. Int. J. Light. Mater. Manuf. 2, 355–361. https://doi.org/10.1016/j.ijlmm.2019.04.001.

Giagnorio, M., Amelio, A., Grüttner, H., Tiraferri, A., 2017. Environmental impacts of detergents and benefits of their recovery in the laundering industry. J. Clean. Prod. 154, 593–601. https://doi.org/10.1016/j.jclepro.2017.04.012.

Gökelma, M., Celik, D., Tazegul, O., Cimenoglu, H., Friedrich, B., 2018. Characteristics of TI6AL4V powders recycled from turnings via the HDH technique. Metals (Basel) 8. https://doi.org/10.3390/met8050336.

Goonan, T.G., 2004. Titanium recycling in the United States in 2004. Flow Stud. Recycl. Met. Commod. United States 1–16.

Hamayun, M.H., Hussain, M., Maafa, I.M., Aslam, R., 2019. Integration of hydrogenation and dehydrogenation system for hydrogen storage and electricity generation – simulation study. Int. J. Hydrogen Energy 44, 20213–20222. https://doi.org/10.1016/j.ijhydene.2019.06.053.

Hu, M., Ji, Z., Chen, X., Wang, Q., Ding, W., 2012. Solid-state recycling of AZ91D magnesium alloy chips. Trans. Nonferrous Metals Soc. China 22, s68–s73. https://doi.org/10.1016/S1003-6326(12)61685-9.

Kassym, K., Perveen, A., 2020. Atomization processes of metal powders for 3D printing. Mater. Today Proc. 26, 1727–1733. https://doi.org/10.1016/j.matpr.2020.02.364.

Konečná, R., Medvecká, D., Nicoletto, G., 2019. Structure, texture and tensile properties of Ti6Al4V produced by selective laser melting. Prod. Eng. Arch. 25, 60–65. https://doi.org/10.30657/pea.2019.25.12.

Kwade, A., 1999. Wet comminution in stirred media mills — research and its practical application. Powder Technol. 105, 14–20. https://doi.org/10.1016/S0032-5910(99)00113-8.

Lagutkin, S., Achelis, L., Sheikhaliev, S., Uhlenwinkel, V., Srivastava, V., 2004. Atomization process for metal powder. Mater. Sci. Eng., A 383, 1–6.

Luo, P., McDonald, D.T., Zhu, S.M., Palanisamy, S., Dargusch, M.S., Xia, K., 2012. Analysis of microstructure and strengthening in pure titanium recycled from machining chips by equal channel angular pressing using electron backscatter diffraction. Mater. Sci. Eng., A 538, 252–258. https://doi.org/10.1016/j.msea.2012.01.039.

Mahboubi Soufiani, A., Enayati, M.H., Karimzadeh, F., 2010. Fabrication and characterization of nanostructured Ti6Al4V powder from machining scraps. Adv. Powder Technol. 21, 336–340. https://doi.org/10.1016/j.apt.2009.12.018.

Mahmood, K., Stevens, N., Pinkerton, A.J., 2012. Laser surface modification using Inconel 617 machining swarf as coating material. J. Mater. Process. Technol. 212, 1271–1280. https://doi.org/10.1016/j.jmatprotec.2012.01.014.

Malỳ, M., Höller, C., Skalon, M., Meier, B., Koutnỳ, D., Pichler, R., Sommitsch, C., Paloušek, D., 2019. Effect of process parameters and high-temperature preheating on residual stress and relative density of Ti6Al4V processed by selective laser melting. Materials (Basel) 16. https://doi.org/10.3390/ma12060930.

Martchek, K.J., 2000. The importance of recycling to the environmental profile of metal products. Proc. TMS Fall Extr. Process. Conf. 4th Intern 19–28. https://doi.org/10.1002/9781118788073.ch2.

de Mendonça, C.S.P., Oliveira, A.F., Oliveira, L.A., da Silva, M.R., de Melo, M.L.N.M., Silva, G., 2018. Structural and magnetic properties of duplex stainless steel (UNS S31803) powders obtained by high energy milling of chips with additions of NbC. Mater. Res. 21 (1), 1–6. https://doi.org/10.1590/1980-5373-MR-2017-0717.

Misiolek, W., Haase, M., Ben Khalifa, N., Tekkaya, A., Kleiner, M., 2012. High quality extrudates from aluminum chips by new billet compaction and deformation routes. CIRP Ann. - Manuf. Technol. 61, 239–242. https://doi.org/10.1016/j.cirp.2012.03.113.

Mittal, M.L., 2010. Estimates of emissions from coal. Fired Thermal Power Plants in India 39, 1–22.

Mohankumar, S., Senthilkumar, P., 2017. Particulate matter formation and its control methodologies for diesel engine: a comprehensive review. Renew. Sustain. Energy Rev. 80, 1227–1238. https://doi.org/10.1016/j.rser.2017.05.133.

Murr, L.E., Esquivel, E.V., Quinones, S.A., Gaytan, S.M., Lopez, M.I., Martinez, E.Y., Medina, F., Hernandez, D.H., Martinez, E., Martinez, J.L., Stafford, S.W., Brown, D.K., Hoppe, T., Meyers, W., Lindhe, U., Wicker, R.B., 2009. Microstructures and mechanical properties of electron beam-rapid manufactured Ti-6Al-4V biomedical prototypes compared to wrought Ti-6Al-4V. Mater. Char. 60, 96–105. https://doi.org/10.1016/j.matchar.2008.07.006.

Naik, S.N., Walley, S.M., 2020. The Hall–Petch and inverse Hall–Petch relations and the hardness of nanocrystalline metals. J. Mater. Sci. 55, 2661–2681. https://doi.org/10.1007/s10853-019-04160-w.

Norgate, T.E., Rajakumar, V., Trang, S., 2004. Titanium and other light metals - technology pathways to sustainable development. Australas. Inst. Min. Metall. Publ. Ser. 105–112.

Paraskevas, D., Vanmeensel, K., Vleugels, J., Dewulf, W., Deng, Y., Duflou, J.R., 2014. Spark plasma sintering as a solid-state recycling technique: the case of aluminum alloy scrap consolidation. Mater. (Basel, Switzerland) 7, 5664–5687. https://doi.org/10.3390/ma7085664.

Pourghahramani, P., 2006. Effects of Grinding Variables on Structural Changes and Energy Conversion during Mechanical Activation Using Line Profile Analysis (LPA) 163.

Prem, G., Ragu, M., Sivakumar, R., Sasidharan, S., 2015. Characterization of Cu Chips Producing through High Energy Ball Milling, pp. 1675–1679.

Rosso, M., Suśniak, M., Dutkiewicz, J., Karwan-Baczewska, J., Actis Grande, M., 2013. Structure investigation of ball milled composite powder based on AlSi5Cu2 alloy chips modified by sic particles. Arch. Metall. Mater. 58, 437–441.

Rotmann, B., Friedrich, B., Lochbichler, C., 2011. Challenges in titanium recycling - do we need a new specification for secondary alloys?. In: Proc. - Eur. Metall. Conf. EMC 2011, vol. 4, pp. 1465–1480.

Sharma, R.K., Sodhi, G.P.S., Bhakar, V., Kaur, R., Pallakonda, S., Sarkar, P., Singh, H., 2020. Sustainability in manufacturing processes: finding the environmental impacts of friction stir processing of pure magnesium. CIRP J. Manuf. Sci. Technol. 30, 25–35. https://doi.org/10.1016/j.cirpj.2020.03.007.

Shrestha, S., Chou, K., 2018. Single track scanning experiment in laser powder bed fusion process. Procedia Manuf. 26, 857–864. https://doi.org/10.1016/j.promfg.2018.07.110.

Singh, M., Dhiman, S., Singh, H., Berndt, C.C., 2020. Optimization of modulation-assisted drilling of Ti-6Al-4V aerospace alloy via response surface method. Mater. Manuf. Process. 35, 1313–1329. https://doi.org/10.1080/10426914.2020.1772487.

Singh, S., Chaudhary, S., Singh, H., 2019. Effect of electroplated interlayers on properties of cold-sprayed copper coatings on SS316L steel. Surf. Coating. Technol. 375, 54–65. https://doi.org/10.1016/j.surfcoat.2019.07.015.

Sopicka-lizer, M., 2010. High-Energy Ball Milling: Mechanochemical Processing of Nanopowders. Woodhead Publishing. https://doi.org/10.1533/9781845699444.1.

Suryanarayana, C., 2001. Mechanical alloying and milling. Prog. Mater. Sci. 46, 1–184. https://doi.org/10.1016/S0079-6425(99)00010-9.

Tekkaya, A.E., Schikorra, M., Becker, D., Biermann, D., Hammer, N., Pantke, K., 2009. Hot profile extrusion of AA-6060 aluminum chips. J. Mater. Process. Technol. 209, 3343–3350. https://doi.org/10.1016/j.jmatprotec.2008.07.047.

Tengzelius, J., Ab, H., Höganäs, S., 2000. Life Cycle Assessment (LCA) of Powder Metallurgy Resources. Press. Sinter. 6.

Townsend, A., Senin, N., Blunt, L., Leach, R.K., Taylor, J.S., 2016. Surface texture metrology for metal additive manufacturing: a review. Precis. Eng. 46, 34–47. https://doi.org/10.1016/j.precisioneng.2016.06.001.

Tsirlis, M., Michailidis, N., 2020. Low-pressure gas atomization of aluminum through a Venturi nozzle. Adv. Powder Technol. 31, 1720–1727. https://doi.org/10.1016/j.apt.2020.02.011.

TU Delft, 2020. Indicator systeem ecocost [WWW Document], 5.8.21, URL. https://www.ecocostsvalue.com/.

Umeda, J., Mimoto, T., Imai, H., Kondoh, K., 2017. Powder forming process from machined titanium chips via heat treatment in hydrogen atmosphere. Mater. Trans. 58, 1702–1707. https://doi.org/10.2320/matertrans.Y-M2017833.

Ünal, A., 1990. Production of rapidly solidified aluminium alloy powders by gas atomisation and their applications. Powder Metall. 33, 53–64. https://doi.org/10.1179/pom.1990.33.1.53.

Vaglio, E., De Monte, T., Lanzutti, A., Totis, G., Sortino, M., Fedrizzi, L., 2020. Single tracks data obtained by selective laser melting of Ti6Al4V with a small laser spot diameter. Data Br 33, 106443. https://doi.org/10.1016/j.dib.2020.106443.

Velasco-Castro, M., Hernández-Nava, E., Figueroa, I.A., Todd, I., Goodall, R., 2019. The effect of oxygen pickup during selective laser melting on the microstructure and mechanical properties of Ti–6Al–4V lattices. Heliyon 5. https://doi.org/10.1016/j.heliyon.2019.e02813.

Velasco-Castro, M., Hernández-Nava, E., Figueroa, I.A., Todd, I., Goodall, R., 2019. The effect of oxygen pickup during selective laser melting on the microstructure and mechanical properties of Ti–6Al–4V lattices. Heliyon 5, e02813. https://doi.org/10.1016/j.heliyon.2019.e02813.

Vogtlander, J., 2010. LCA-based Assessment of Sustainability: the Eco-costs/Value Ratio EVR.

Weber, H.J., 1961. Air pollution problems of the foundry industry. J. Air Pollut. Control Assoc. 11, 157–172. https://doi.org/10.1080/00022470.1961.10467985.

Wiedmann, T.O., Schandl, H., Lenzen, M., Moran, D., Suh, S., West, J., Kanemoto, K., 2015. The material footprint of nations. Proc. Natl. Acad. Sci. Unit. States Am. 112, 6271–6276.

Wilson, B.P., Lavery, N.P., Jarvis, D.J., Anttila, T., Rantanen, J., Brown, S.G.R., Adkins, N.J., 2013. Life cycle assessment of gas atomised sponge nickel for use in alkaline hydrogen fuel cell applications. J. Power Sources 243, 242–252. https://doi.org/10.1016/j.jpowsour.2013.05.186.

Xu, H., Zou, N., Li, Q., 2017. Effect of ball milling time on microstructure and hardness of porous magnesium/carbon nanofiber composites. JOM 69, 1236–1243. https://doi.org/10.1007/s11837-017-2361-3.

Zegzulka, J., Gelnar, D., Jezerska, L., Ramirez-Gomez, A., Necas, J., Rozbroj, J., 2018. Internal friction angle of metal powders. Metals (Basel) 8, 1–12. https://doi.org/10.3390/met8040255.

Zhang, Ying, Lu, W., Sun, P., Fang, Z.Z., Qiao, S., Zhang, Yi, Zheng, S., 2020. Deoxygenation of Ti metal: a review of processes in literature. Int. J. Refract. Metals Hard Mater. 91, 105270 https://doi.org/10.1016/j.ijrmhm.2020.105270.